Available online at www.sciencedirect.com
ScienceDirect
Computer Physics Communications 179 (2008) 107–111
Computer Physics Communications
www.elsevier.com/locate/cpc

Numerical simulation of field emission efficiency of anodic aluminum oxide carbon nanotube field emitter in the triode structure

Yiming Li *, Hui-Wen Cheng

Department of Communication Engineering, National Chiao Tung University, Hsinchu 300, Taiwan

Available online 30 January 2008

Abstract

In this work, we study the field emission (FE) properties of carbon nanotubes (CNTs) field emitter in the triode structure fabricated with anodic aluminum oxide (AAO) template. To obtain the self-consistent solution, a set of two-dimensional Maxwell's equations coupling with Lorentz equation are solved with a finite difference time domain (FDTD) particle-in-cell (PIC) method. The FE current is then computed with the Fowler–Nordheim equation. Calculated result of the collected current density shows good agreement with the measured data for the fabricated sample. Effect of the height and number of CNTs on the collected electron current density is thus investigated. We find that the explored structure with few number of CNTs exhibit high current density due to insignificant screening effect. The current density is low and approaches to stable current level when the number of CNTs increases. The simulation further predicts that the structure with the height of CNTs = 0.42 μm has a maximum current density. The FE efficiency (i.e., the collected electron current density/the emission current density) versus the number of CNTs is estimated. The explored AAO-CNTs triode structure maintains high FE efficiency (∼95%) with a nonzero gate voltage.

PACS: 81.15.Gh; 81.16.-c; 52.20.-j; 52.25.-b; 61.46.+w

Keywords: Carbon nanotubes; Triode structure; Anodic aluminum oxide; Field emission; Maxwell's equations; Fowler–Nordheim equation; Numerical simulation; FDTD-PIC

1. Introduction

Carbon nanotubes (CNTs) are promising in cold-cathode flat panel displays for their chemical stability, mechanical strength, and electron emission properties [1–7]. To pursue highly uniform emitted and collected currents, it is necessary to grow vertically aligned arrays of CNTs on a large area with suitable tube density and size. Various template-fabrication methods have been reported [8,9]; in particular, anodic aluminum oxide (AAO) nanotemplates because AAO has vertical pore channels, highly ordered pore arrangement, and uniform pore size [9]. A self-consistent investigation on the filed emission (FE) property will benefit the design and fabrication of AAO-CNTs in the triode structure. Unfortunately, study on the FE properties of AAO-CNTs has not been drawn yet.

In this work, new FE triode arrays with the AAO template CNTs as the field emitters are successfully fabricated and analyzed. Fabrication of AAO-CNTs is using standard integrated circuit processes [9]. Finite-difference time domain (FDTD) particle-in-cell (PIC) numerical simulation is developed to examine the FE property [10,11] and current in the CNTs triode structure with the AAO template. The current is computed with the Fowler–Nordheim (FN) equation. Electrons emitted from CNTs at a gate voltage (V_G) are accelerated by an anode voltage (V_A). To validate the numerical simulation, we first calibrate the accuracy of the simulated electron current with the experimental data for (V_A) ranging from 0 to 1000 V. According to our calibration, simulated data shows good agreement with the measured electron current of the AAO-CNTs in the triode structure. We thus explore the effect of the height and number of the CNTs on the FE properties of AAO-CNTs in the triode structure. Using the definition of FE efficiency (i.e., the collected electron current density/the emission current density), the FE efficiency versus the number of CNTs is estimated.

* Corresponding author.
E-mail address: ymli@faculty.nctu.edu.tw (Y. Li).

0010-4655/$ – see front matter
doi:10.1016/j.cpc.2008.01.026

This paper is organized as follows. In Section 2, we illustrate the fabricated AAO-CNTs in the triode structure and state the computational model including FDTD-PIC method. In Section 3, we present the results and discussion. Finally, we draw the conclusions.

2. Computational model

Fig. 1 (a)–(c) shows SEM images of the fabricated samples [9]. Plot of Fig. 1(b) is an enlarged image of Fig. 1(a). The image, shown in Fig. 1(c), is a vertically cross-sectional view of SEM. The CNT emitters are grown in an ECR-CVD system at 600 °C, and the CNTs grow along the axis of pore channels and have a tube diameter compliant with the pore size of the AAO pore channels, resulting in uniform diameter and well-aligned emitters, as shown in Fig. 1 (a) and (b). An Al film thick is deposited on the silicon wafer, and the AAO pore channel array is subsequently prepared by electrochemical anodization in oxalic acid solution at 21 °C under a constant polarization voltage of 40 V. AAO pore channel array has highly ordered pore arrangement with a uniform pore size of 70–80 nm and the length of the vertical pore channel is about 700 nm [9].

With the symmetrical property of fabricated AAO-CNTs in the triode structure, as shown in Fig. 1(b), a two-dimensional (2D) FDTD-PIC numerical simulation is developed to investigate the emitted and collected electron currents of the structure, where the currents are computed with the FN equation. The Maxwell's equations in an isotropic medium are:

$$\frac{\partial B}{\partial t} + \nabla \times E = 0, \tag{1}$$

$$\frac{\partial D}{\partial t} - \nabla \times H = J, \tag{2}$$

$$F = q_i\big(E(x_i) + v_i \times B(x_i)\big), \tag{3}$$

$$\frac{\partial x_i}{\partial t} = v_i, \tag{4}$$

$$B = \mu H, \qquad D = \epsilon E, \tag{5}$$

where E and B are the electric and magnetic fields, x_i is the position of charge particle, and J and ρ are the current density and charge density resulting from charge particles, and μ and ϵ are permeability and permittivity. For the simulation domain, shown in Fig. 1(d), the equations above are subject to constraints provided by Gauss's law and the corresponding rule for the divergence of B,

$$\nabla \cdot E = \frac{\rho}{\epsilon}, \qquad \nabla \cdot B = 0. \tag{6}$$

These equations are solved with a free-space boundary for absorb outgoing waves. Direct integration of Maxwell's equations allows us to determine the dynamic behavior of electromagnetic systems. When there are electrically charged particles present, the relativistic equations of motion based on the Lorentz force can also be integrated directly to include the effects of charge and current density. Integration of the Maxwell's and Lorentz equations solves any classical electromagnetic problems involving electromagnetic fields and induced forces. We use PIC method coupled with the FE model to simulate the electron emission of AAO-CNTs in the triode structure. The electromagnetic PIC steps are performed in the numerical simulation, as shown in Fig. 2. Starting from a specified initial state, we simulate electrostatic fields as its evolution in time. We then perform a time integration of Faraday's law, Ampere's law, and the relativistic Lorentz equation.

The full set of Maxwell's time-dependent equations above is simultaneously solved to obtain electromagnetic fields. Sim-

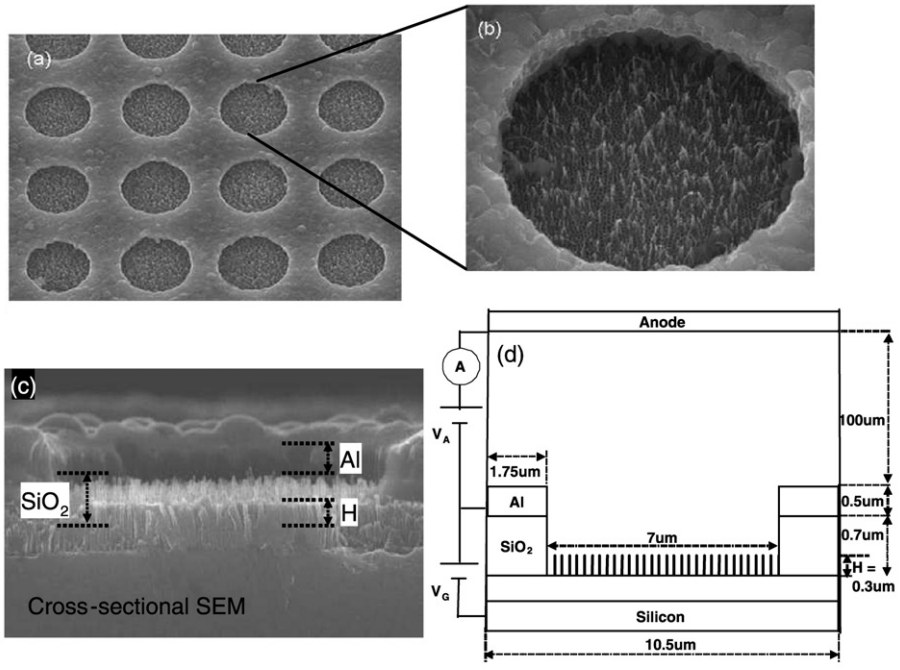

Fig. 1. (a) The SEM image of the AAO-CNTs triode array. (b) An enlarged SEM image of a single triode. (c) A cross-sectional SEM of the fabricated sample. (d) The simulation domain of the AAO-CNTs in the triode structure [9].

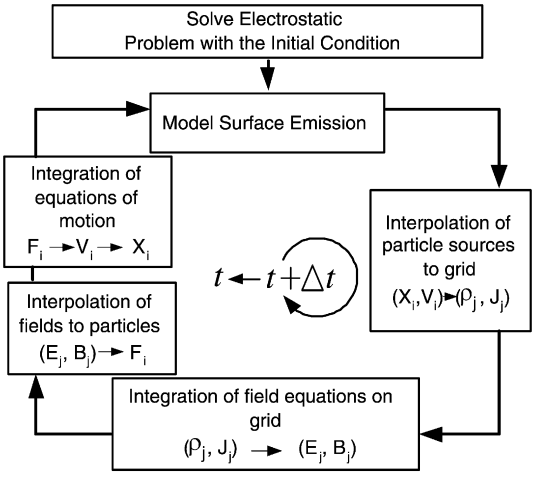

Fig. 2. A simulation flow for the FDTD-PIC scheme.

ilarly, the Lorentz force equation is solved to obtain relativistic particle trajectories. In addition, the electromagnetic fields are advanced in time at each time step. The charged particles are moved according to the Lorentz equation using the fields advanced in each time step. The weighted charge density and current density at the grids are subsequently calculated. The obtained charge density and current density are successively used as sources in the 2D Maxwell's equations for advancing the electromagnetic fields. These steps are repeated for each time step until the specified number of time steps is reached. We notice that the space-charge effects are automatically included in the simulation algorithms. This computational scheme thus approaches to self-consistent simulation of the electromagnetic fields and charged particles. In the FE process, the electron emission is calculated by the FN equation,

$$J = \frac{AE^2}{\varphi t^2} \exp\left(\frac{-Bv(y)\varphi^{3/2}}{E}\right), \tag{7}$$

where $A = 1.541 \times 10^{-6}$ A eV/V^2 and B (V μm^{-1}) is a fitting parameter, E is the normal component of the electric field at the emitter surface. φ is the work function of the emission material, $t^2 \approx 1.1$, and $v(y) = 0.95 - y^2$ with $y = 3.79 \times 10^{-5} \times E^{1/2}/\varphi$ is in SI unit. The emission current density is determined by Eq. (7) according to the local electric field, the work function of emitter material, and the geometric factors. We notice that, in the entire simulation, all dimensions of physical quantities are the same with the experimental settings.

3. Results and discussion

The accuracy of the FDTD-PIC simulation is justified firstly, as shown in Fig. 3. We calibrate the simulated (dots) electron current with the experimental (line) data for the sample, where $V_A = 1000$ V and $V_G = 0$ V. The simulation is a time-domain calculation, so we calibrate data every 5 V for V_A ranging from 0 to 1000 V. The inset of Fig. 3 shows the parameter B which increases when V_A increases. Using the calibrated simulation model, we now explore the FE property due to the density and morphology of the deposited CNTs.

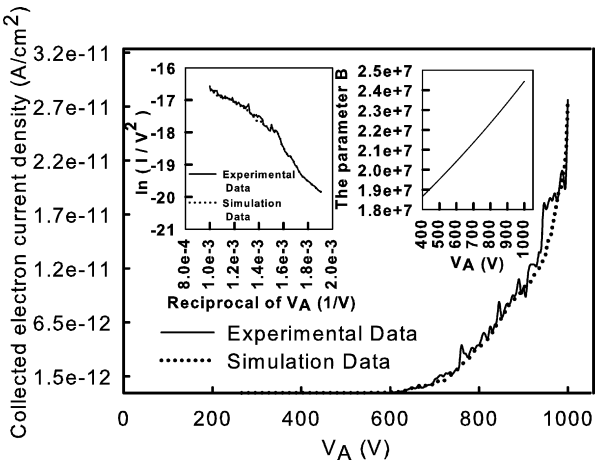

Fig. 3. Comparison between the simulation (dots) and measurement (line) of the collected electron current for the structure with 30 CNTs and the height = 0.3 μm. The left inset is the corresponding F-N plot. The right inset is the parameter B versus the applied voltage.

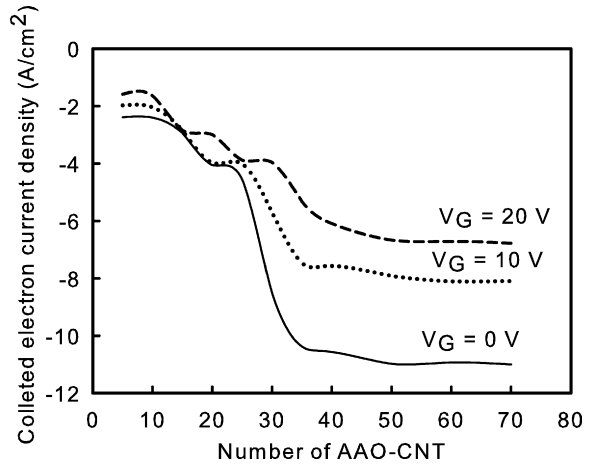

Fig. 4. The predicted electron current density (in Log scale) versus the number of CNTs with different V_G, where $V_A + V_G = 1000$ V.

We find that the structure with less than 10 CNTs exhibits high electron current density when the number of CNTs varies from 1 to 70, as shown in Fig. 4. It is because that the structure with few CNTs results in strong electric field for the case of $V_G = 0$ V. For different V_G, we have similar estimation on the effect of the number of CNTs on the collected electron current. The collected electron current is sensitively affected when the number of CNTs is increased due to the evident screening effect. The FE property is further suppressed when the number of CNTs > 30. The electric field of the structure with 10 CNTs (not shown here) is stronger than that of 30 CNTs, as shown in Fig. 5, even we have more concentrated electron trajectory for the structure with 30 CNTs. It is because the AAO-CNTs with high density CNTs will results in the strong screening effect among adjacent emitters and thus reduce the magnitude of electric field, consequently, the emitted electrons attracted by anode will be fewer, as listed in Table 1.

We also study the variation of the electron current of the AAO-CNTs in the triode structure. By uniformly changing the height of CNTs from 0.27 to 0.48 μm, the simulation further

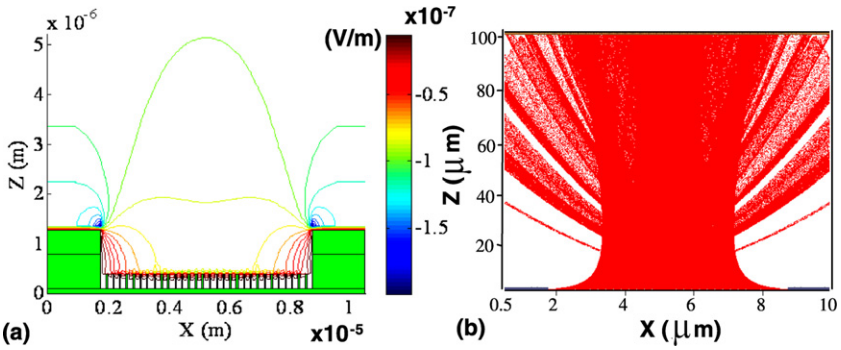

Fig. 5. (a) The electric field of the AAO-CNTs in the triode structure with 30 CNTs. (b) The electron trajectory of the AAO-CNTs in the triode structure with 30 CNTs.

Table 1
The magnitude of electric field and collected electron current density for the structure with 10, 15, 20, and 30 CNTs

Number of CNTs	10	15	20	30
E (10^6 V/m)	11.107	9.067	8.795	5.987
I (10 nA/cm^2)	63.68	6.751	1.165	0.0642

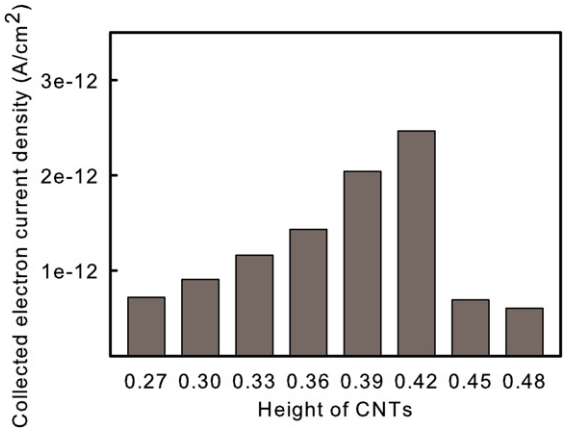

Fig. 6. The simulated electron current of the AAO-CNTs versus the height of CNTs, where $V_A = 1000$ V and $V_G = 0$ V.

predicts that there is an optimal height $(H) = 0.42$ μm so that the explored structure, shown in Fig. 1(d), exhibits high electron current density among cases, as shown in Fig. 6, where $V_A = 1000$ V and $V_G = 0$ V.

The electron current depends upon the height of CNTs (about 3-times variation). The selection of the height of CNTs is limited by the height of $SiO_2 = 0.7$ μm, as shown in Fig. 1(d). A maximal electron current could be obtained when the height of CNTs is approximately equal to 0.6 times the height of SiO_2. The FE efficiency will be lower, when the number of CNTs is increasing, where $V_G = 0$ V, as shown in the left plot of Fig. 7. The FE efficiency ~95% when the structure with less than ~40 CNTs, where $V_A + V_G = 1000$ V, $V_G = 10$ V, as shown in the right one of Fig. 7. Adding gate voltage will focus the emission beam. Therefore, the anode will collected more electrons. If the number of CNTs > 40, the strength of electric filed is reduced due to strong screening effect and thus result in low (~70%) FE efficiency. For $V_G = 0$ V, the structure is right the diode one, and the FE efficiency becomes low, compared with the result of triode structure.

4. Conclusions

In this paper, we have applied a 2D FDTD-PIC simulation to explore the FE property of the fabricated AAO-CNTs in the triode structure. The structure with few number of CNTs ex-

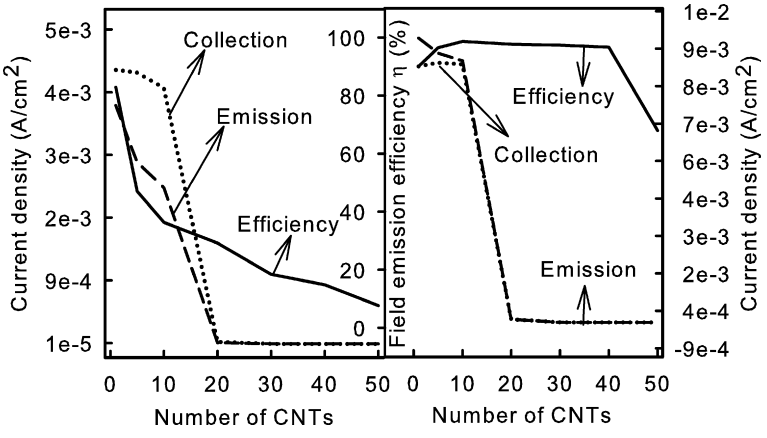

Fig. 7. The emitted and collected electron current density and the FE efficiency versus the number of CNTs, where the left plot is under $V_A = 1000$ V and $V_G = 0$ V, the right plot is under $V_A + V_G = 1000$ V and $V_G = 10$ V. I_a is the electron current collected on the anode, I_e is the emission current.

hibits high emission current density when the number of CNTs ranges from 1 to 70 due to strong electric filed. However, the uniformity of current density may have a large amount fluctuation for the structure with few CNTs (e.g., <10 CNTs), which complicates the fabrication of AAO-CNTs triode structure. By uniformly changing the height of CNTs from 0.27 to 0.48 μm, the structure with the height $= 0.42$ μm has high emission current density among cases. Optimal efficiency ($\sim$95%) is when the structure with less than $\sim$40 CNTs. We are currently exploring the effect of the diameter and position of CNTs on the FE properties with full 3D approach.

Acknowledgements

This work was supported in part by Taiwan National Science Council (NSC) under Contract NSC-96-2221-E-009-210 and Contract NSC-95-2752-E-009-003-PAE, and by the Chunghwa Picture Tubes under a 2006-2008 grant. Measurement data from Professor Dr. Fu-Ming Pan is gratefully acknowledged.

References

[1] Y. Saito, S. Uemura, Field emission from carbon nanotubes and its application to electron sources, Carbon 38 (2000) 169–182.

[2] Y. Huh, J.Y. Lee, J.H. Lee, T.J. Lee, S.C. Lyu, C.J. Lee, Selective growth and field emission of vertically well-aligned carbon nanotubes on hole-patterned silicon substrates, Chem. Phys. Lett. 375 (2003) 388–392.

[3] W.A. de Heer, A. Chatelain, D. Ugarte, A carbon nanotube field emission electron source, Science 270 (1995) 1179–1180.

[4] K.A. Dean, B.R. Chalamala, The environmental stability of field emission from single-walled carbon nanotubes, Appl. Phys. Lett. 75 (1999) 3017–3019.

[5] Q.H. Wang, T.D. Corrigan, J.Y. Dai, R.P.H. Chang, A.R. Krauss, Field emission from nanotube bundle emitters at low field, Appl. Phys. Lett. 70 (1997) 3308–3310.

[6] M. Huhtala, A. Kuronen, K. Kaski, Computational studies of carbon nanotube structures, Comput. Phys. Comm. 147 (2002) 91–96.

[7] X. Sua, L. Zhanga, W. Lei, X. Zhang, Study of the influence of the dielectric layer thickness in a CNT-FED, Ultramicroscopy 107 (2007) 844–848.

[8] P.-L. Chen, C.-T. Kuo, T.-G. Tsai, B.-W. Wu, C.-C. Hsu, F.-M. Pan, Self-organized titanium oxide nanodot arrays by electrochemical anodization, Appl. Phys. Lett. 82 (2003) 2796–2798.

[9] C.-C. Lin, K.-C. Chang, F.-M. Pan, C.-T. Kuo, M. Liu, C.-N. Mo, Growth of carbon nanotube field emitters in the triode structure using anodic aluminum oxide as th template, Diamond and Related Materials 16 (2007) 1388–1392.

[10] Y. Li, H.-Y. Chao, H.-Y. Lo, High field emission efficiency surface conduction electron emitters, J. Comput. Electron. (2008), doi:10.1007/s10825-007-0168-0.

[11] H.-Y. Lo, Y. Li, H.-Y. Chao, C.-H. Tsai, F.-M. Pan, Field emission properties of palladium surface conduction electron-emitter, Nanotechnology 18 (2007) 571–577.